Supporting Information

In situ analysis of liposome hard and soft protein corona structure and composition in a single label-free workflow

Otto K. Kari*[a,b], Joseph Ndika[c], Petteri Parkkila[b], Antti Louna[a], Tatu Lajunen[a], Anne Puustinen[d], Tapani Viitala*[b†], Harri Alenius[c,e] and Arto Urtti[a,f]

Table of contents

List of additional supplementary files

Table M1: Biophysical analysis replicate data calculations.
Table P1: All differentially enriched or depleted proteins with their relative fold-changes in abundance.
Table P2: Formulation-dependent differences in proteins enriched or depleted in hard versus soft corona.
Table P3: Formulation-dependent changes in soft corona (SC) protein abundance.

Raw proteomics data and/or MaxQuant output files are available upon reasonable request from the corresponding author(s).

Supplementary information for MP-SPR biophysical analysis: theory of the effective thickness calculations

Assuming homogeneous layer morphology, the general Jung model equation[1] for the change in the peak angular minimum (SPR response) is

$$R = S(n - n_b)\left(1 - e^{-d/\delta}\right) \quad \text{(Eq. S1)}$$

As per the formalism developed by Rupert *et al.*[2], the SPR response from liposomes covering the sensor surface can be written as

$$R = S\left(\mathrm{d}n/\mathrm{d}C_*\right)cc_*(\pi dl)\left(1 - e^{-d/\delta}\right). \quad \text{(Eq. S2)}$$

The parameters are described as follows:
S: sensitivity constant of the sensor for the changes in bulk refractive index (degrees)
$(\mathrm{d}n/\mathrm{d}C_*)$: refractive index increment. For lipids[3], $(\mathrm{d}n/\mathrm{d}C_*)_l \approx 0.135$ cm^3/g and for protein[4], $(\mathrm{d}n/\mathrm{d}C_*)_p \approx 0.185$ cm^3/g.
n: refractive index of the layer
n_b: refractive index of the bulk liquid
c: number density of nanoparticles on the surface (nanoparticles per area)
c_*: effective density of the layer forming the nanoparticle
d: diameter of the nanoparticle
l: thickness of the layer forming the nanoparticle, i.e. (effective) thickness of the lipid bilayer or the protein corona.
δ: decay length of the evanescent electric field above the sensor surface

1. The parameters S and δ for the two wavelengths were calculated for a single sensor by determining the theoretical peak angle minima in the Fresnel layer modeling for $n = 1.34$, 1.35 and 1.36 at different values of layer thickness. Equation S1 was fitted to these datasets and average best fit parameters from these three refractive indices were taken.

2. All possible influences of absorbance of the ICG liposomes and the changes in bulk refractive index during the plasma flow must be considered in the modelling. Absorbance of ICG causes a shift in the peak minimum intensity of the SPR reflectance curve. This was first modelled by using imaginary part of the refractive index (k in $n + ik$) in the Fresnel layer modeling, after which the k was changed to zero, and the new peak positions were determined from the modeled reflectance curves. Similarly, the change in bulk refractive index during the plasma injection was first modeled by using the angle of total internal reflection to calculate the changes in bulk refractive indices. Then, bulk refractive indices were changed to their original values (background buffer) and the new bulk-corrected response values were determined from the modelled reflectance curves.

3. Diameters of the non-ICG liposomes were estimated using the ratio of responses of two wavelengths (1 = 670 nm, 2 = 785 nm):

$$\frac{R_1}{R_2} = \frac{S_1}{S_2}\frac{(\mathrm{d}n/\mathrm{d}C_*)_1}{(\mathrm{d}n/\mathrm{d}C_*)_2}\frac{\left(1-e^{-d/\delta_1}\right)}{(1-e^{-d/\delta_2})} \quad \text{(Eq. S3)}$$

where $\frac{(\mathrm{d}n/\mathrm{d}C_*)_1}{(\mathrm{d}n/\mathrm{d}C_*)_2} \approx 1.02$ for non-absorbing liposomes[2]. For ICG liposomes, the thickness was obtained from the Fresnel layer modeling, since unique solutions of d, n and k could be calculated.

4. Since the number densities of protein and liposomes are assumed equal (one protein corona coats one liposome), using Eq. S2, we arrive at

$$c_p = c_l \Rightarrow \quad \text{(Eq. S4)}$$
$$\frac{R_p}{R_l} = \frac{(\mathrm{d}n/\mathrm{d}C_*)_p}{(\mathrm{d}n/\mathrm{d}C_*)_l}\frac{\left(1-e^{-d_p/\delta}\right)}{(1-e^{-d_l/\delta})}\frac{c_{*,p}}{c_{*,l}}\frac{d_p}{d_l}\frac{l_p}{l_l}$$

It was noticed that it is not possible to determine the accurate diameter of the liposomes with the protein corona, for deducing the change in nanoparticle diameter (using Eq. S3). Therefore, we assume that the change in diameter can be written as $d_p \approx d_l + l_p$ in the equation above. Then the Taylor expansion of the diameter-dependent factor ($l_p \ll d_l$) in the above relationship can be written as

$$\frac{d_l}{(d_l+l_p)}\frac{\left(1-e^{-d_l/\delta}\right)}{\left(1-e^{-(d_l+l_p)/\delta}\right)} \approx 1 + l_p\left(\frac{1}{\delta(1-e^{d_l/\delta})} - \frac{1}{d_l}\right) = 1 + l_p\varphi(d_l). \quad \text{(Eq. S5)}$$

This allows to solve l_p:

$$l_p = \left(\frac{R_l}{R_p}\frac{(\mathrm{d}n/\mathrm{d}C_*)_p}{(\mathrm{d}n/\mathrm{d}C_*)_l}\frac{c_{*,p}}{c_{*,l}l_l} - \varphi(d_l)\right)^{-1}, \quad \text{(Eq. S6)}$$

where $c_{*,p} = \alpha_p\rho_p \approx 0.54 \cdot 1.35\ \mathrm{g/cm^3} = 0.729\ \mathrm{g/cm^3}$ is the effective density of the protein layer considering random close packing of equal spheres on the liposome surface. A reasonable thickness of $l_l =$ 5 nm and density of $c_{*,l} = 1.05$ g/cm^3 for the lipid bilayer was used. Data for the 670 nm wavelength was used in analysis.

5. Since surface mass density for a hollow sphere is defined as $\Gamma = cc_*(\pi d^2 l)$, Eq. S2 can be used to solve the surface mass densities of the liposomes and protein,

$$\Gamma = \frac{R}{S(\mathrm{d}n/\mathrm{d}C_*)(1-e^{-d/\delta})} \times d. \quad \text{(Eq. S7)}$$

Surface mass densities for protein were calculated using the thickness $d_p \approx d_l + l_p$ with the effective thickness calculated using Eq. S6.

There is an alternative approach to arrive to the equation for effective thickness of the protein corona. Number of lipids in a single liposome is

$$N_l = N_A\frac{\Gamma_{*,l}}{M_l}\pi d_l^2 \quad \text{(Eq. S8)}$$

where $N_A = 6.022 \cdot 10^{23}\ \mathrm{mol}^{-1}$ is the Avogadro constant and M_l is the molar mass of lipids. Since the fraction of protein per lipid is $(\Gamma_p M_l)/(\Gamma_l M_p)$ (Eq. S9), number of protein coating the single liposome is

$$N_p = N_A \Gamma_{*,l} \pi d_l^2 \frac{\Gamma_p}{\Gamma_l M_p}. \quad \text{(Eq. S10)}$$

If one protein is modeled as a particle with volume $V_p = M_p/(N_A \rho_p)$, fractional volume occupied by protein is

$$\alpha_p = \frac{N_p V_p}{\pi d_p^2 l_p} = \frac{\Gamma_p}{\Gamma_l} \frac{\Gamma_{*,l}}{\rho_p l_p} = \frac{\Gamma_p}{\Gamma_l} \frac{d_l^2 c_{*,l} l_l}{d_p^2 \rho_p l_p}. \quad \text{(Eq. S11)}$$

Combining Eq. S11 with Eq. S7 for lipid and protein leads to Eq. S4. The obtained values for the effective thickness can be compared to the estimated effective diameter of a single protein layer,

$$2r\alpha = \sqrt[3]{\frac{6 M_p \alpha^3}{\pi \alpha_p \rho_p N_A}} \quad \text{(Eq. S12)}$$

6. The ratio of protein to lipid can be calculated using Eq. S7:

$$r = \frac{\Gamma_p}{\Gamma_l} \frac{M_l}{M_p} = \frac{R_p}{R_l} \frac{M_l}{M_p} \frac{d_l + l_p}{d_l} \frac{(\mathrm{d}n/\mathrm{d}C_*)_l}{(\mathrm{d}n/\mathrm{d}C_*)_p} \frac{\left(1 - e^{-d_l/\delta}\right)}{\left(1 - e^{-(d_l + l_p)/\delta}\right)}$$
$$\approx \frac{R_p}{R_l} \frac{M_l}{M_p} \frac{(\mathrm{d}n/\mathrm{d}C_*)_l}{(\mathrm{d}n/\mathrm{d}C_*)_p} \left(1 + \frac{l_p}{d_l}\right)^2 \left(1 + l_p \varphi(d_l)\right)$$

The average values for molar mass of protein were 65.5 kg/mol for SC and 76.8 kg/mol for HC, corresponding to effective protein monolayer thickness of 2.9 and 3.1 nm, respectively. Molar mass of 0.8 kg/mol was used for lipids when calculating the ratio of protein to lipid.

Supplementary results and figures

Sensor functionalization and characterization

The hydrophilic self-assembled monolayer (SAM) surface of thiol-grafted pTHMMAA with hydrophobic decylamine anchors (pTHMMAA-BDA) *via* bromoacetic linkers was developed to form liposome layers on the sensor without rupturing them into planar membrane surfaces, while reducing protein binding directly on the sensor (**Figure S1** and **Figure S2**). Successful functionalization was confirmed by PM-IRRAS measurements and DOPC-liposome binding studies with QCM that confirmed immobilization as truncated liposomes (**Figure S3** and **Figure S4**). These sensors can be produced overnight and stored dried at +4°C. The same sensor could be used for the same formulation up to three times following rejuvenation (washing with CHAPS surfactant solution, ethanol and water), stored at +4°C in between measurements immersed in CHAPS (**Figure S5**).

As described in Methods, gold-plated SPR102-AU sensor chips (BioNavis Ltd., Tampere, Finland) were cleaned by boiling for 5 min in H_2O_2:NH_3:H_2O (volume ratios 1:1:5) and washing with Milli-Q water (Merck KGaA, Darmstadt, Germany). Adapting a protocol described earlier[5], the sensors were immersed in 0,2 mg/ml pTHMMAA (synthesized according to Albers *et al.*[6]) in a solution of 99,5% (w/w) ethanol (Altia Oyj, Rajamäki, Finland) and Milli-Q water (8:2) to form a self-assembled monolayer (SAM) by a thiol-*graft-to*-gold reaction

at room temperature for 1 day. The SAM-surfaces were flushed with Milli-Q and ethanol 70% (w/w), and dried with N_2 (g) (Oy Aga Ab, Espoo, Finland). The SAM pTHMMAA *tris*-ends were activated by 1M bromoacetic acid (Merck KGaA) in 2M NaOH (Honeywell Riedel-de-Haën, Morris Plains, NJ, USA) for 15 min, followed by 10 min in 80 mg/ml EDC (Merck KGaA) and 20 mg/ml NHS (Merck KGaA) in sodium diphosphate buffer (Honeywell Fluka, Morris Plains, NJ, USA). The sensors were immersed for 10 min in 30 mg/ml decylamine suspension and treated for 1 min with 1M 2-aminoethanol (pH~8,5). The functionalized pTHMMAA-BDA sensors were washed and dried as described earlier and stored at 4 °C.

The successful functionalization of gold-plated SPR102-AU sensor chips with pTHMMAA followed by bromoacetic acid and decylamine treatments was verified by PM-IRRAS measurements (**Figure S3**). The PM-IRRAS measurements were conducted using a KSV NIMA PM-IRRAS infrared spectrometer (Biolin Scientific, Espoo, Finland). A measurement duration of 300 s using background spectra, sigma and delta magnifications of 2 and 10, respectively, a pre-delta gain of 10, and without pruning in Mertz calculation were used, while the FFT window function was set to hamming with a length of 4096 in both directions. The PM-IRRAS data was analysed using IRRAS 1.0.6 software (Biolin Scientific).

To optimize the reaction conditions, pTHMMAA and bromoacetic acid reactions were carried out with different incubation times from 15 minutes to 36 hours. However, QCM measurements demonstrate that prolonging the reaction time from 15 minutes does not improve liposome binding to the functionalized sensor (Figures S 3, S 4, and S 5). Therefore, only results for 15 min are presented. Since dF > 25 Hz and the overtones do not overlap in Figure S3, the immobilized liposomes retain their spherical shape on the sensor, as opposed to a continuous lipid bilayer[5]. Gold Q-sense (Biolin Scientific) sensors were used for the QCM measurements, functionalized with a procedure identical to the SPR sensors, and measured on KSV QCM-Z500 impedance-based QCM (Biolin Scientific) using an Ismatec ISM596D digital peristaltic pump (Cole-Parmer GmbH).

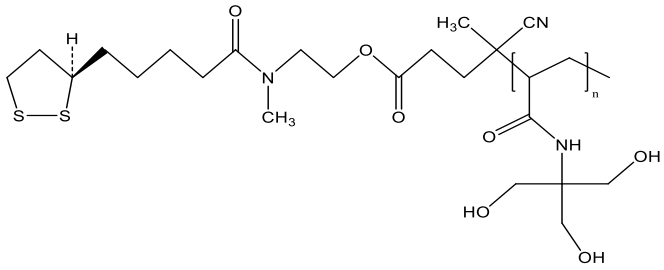

Figure S1. pTHMMAA (poly-*N*-[tris(hydroxy-methyl)methyl]acrylamide)[6,7]. The bulky and highly hydrophilic TRIS headgroups limit interactions between proteins and the polymer core.

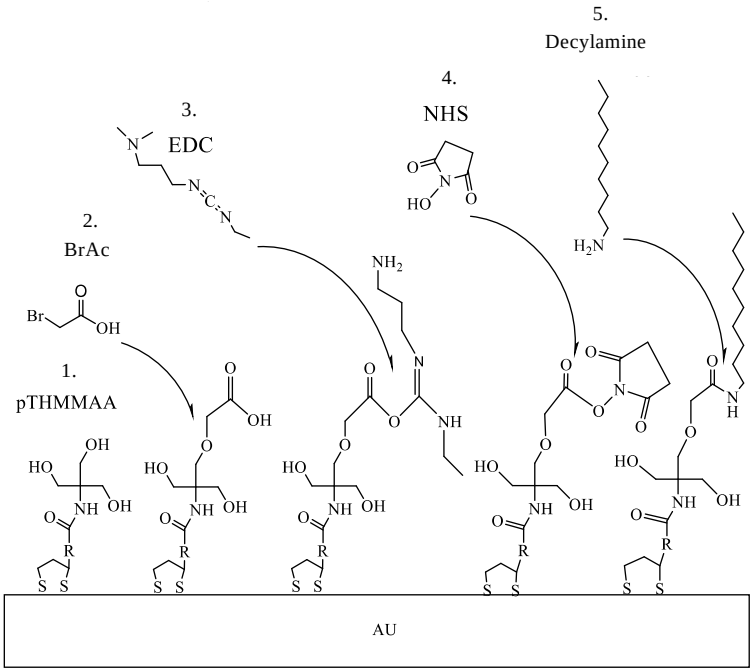

Figure S2. Sequential synthesis of pTHMMAA sensors. Acronyms: pTHMMAA (poly-*N*-[tris(hydroxy-methyl)methyl]acrylamide); BrAc: bromoacetic acid; EDC: N-(3-Dimethylaminopropyl)-N'-ethylcarbodiimide; NHS: N-Hydroxysuccinimide

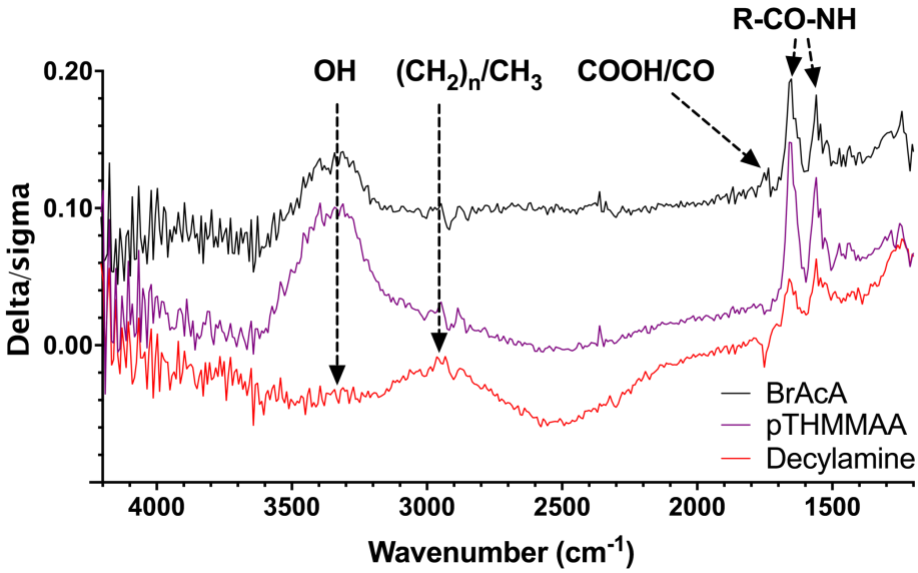

Figure S3. PM-IRRAS spectra to confirm gold-plated biosensor functionalization: pTHMMAA, bromoacetic acid (BrAcA), and decylamine. Spectral peaks corresponding to relevant functional groups have been indicated.

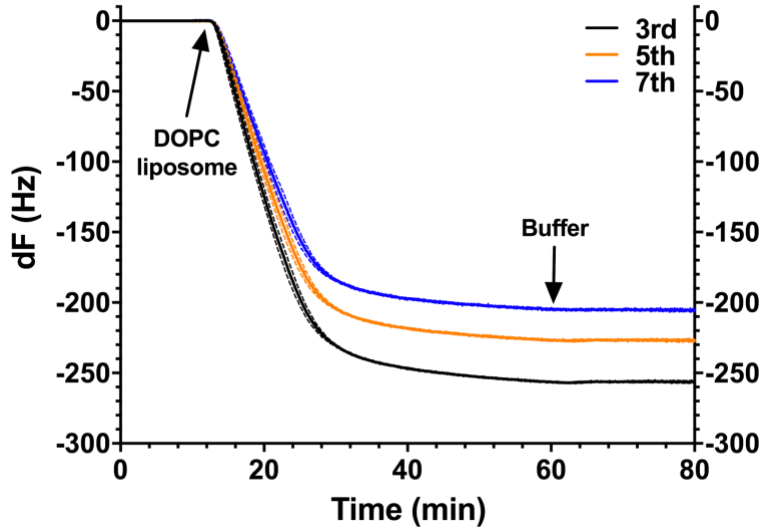

Figure S4. QCM frequency spectra for the 3rd, 5th and 7th harmonics normalized to overtone, with mean in solid and corresponding SD with dashed lines: DOPC liposome binding to pTHMMAA-bromodecylamine functionalized gold QCM sensors treated for 15 min with bromoacetic acid. The magnitude of the change and the non-overlap of the different frequencies indicate the liposomes adsorb to the sensor as spherical vesicles instead of opening into lipid bilayers. The liposomes remain on the sensor after restoration of buffer flow.

Sensor quality control

Olaru *et al.* have suggested that degradation of the L1 chip and other similar sensors in repeated use can be judged based on a specific section of the SPR curve, more specifically the curve shape from peak minimum intensity towards higher angular values[8]. Despite the diminishing binding capacity and surface residue – an expected trade-off in repeated use – the initial SPR curve profiles of the pTHMMAA-BDA sensors shows only limited signs of degradation over three runs (**Figure S5**). The measurements suggests that sensor functionalization remained intact, a beneficial property when the curve shape is a key criterion for accurate modelling using full SPR curves in the angular range of 60-78 degrees.

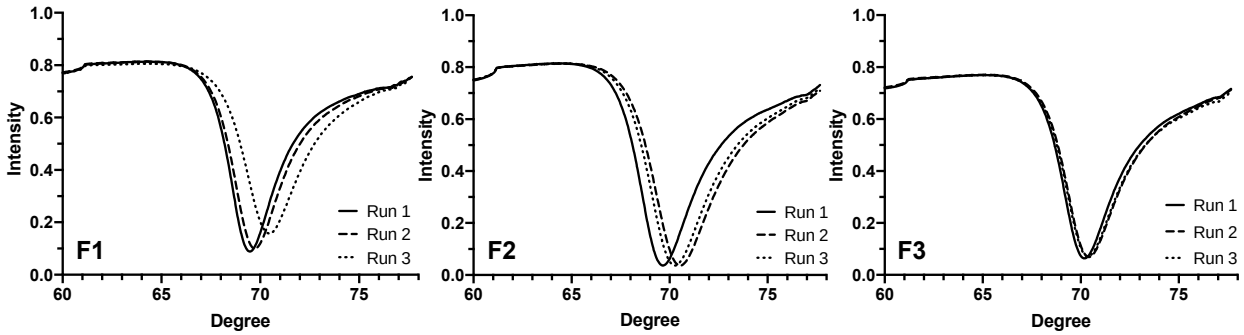

Figure S5. SPR curves for pTHMMAA-BDA sensors 1 minute before liposome immobilization for all three runs (670 nm, channel 1). No signs of sensor degradation can be seen. F1: (+)ICG (-)PEG; F2: (+)ICG (+)PEG; F3: (-)ICG (+)PEG.

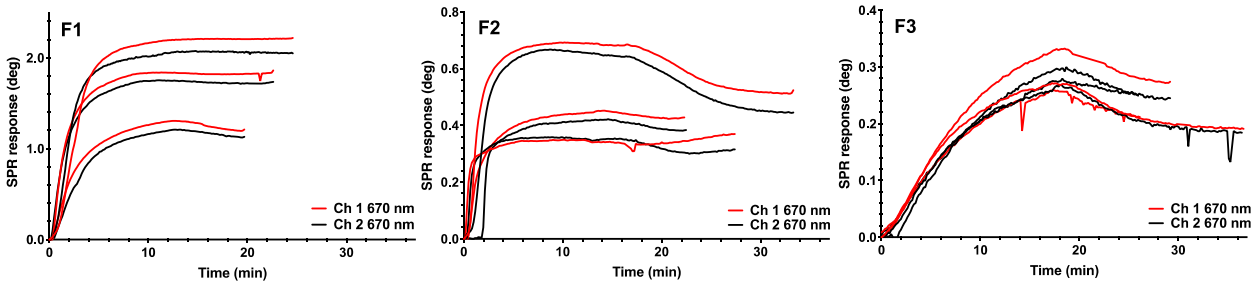

Figure S6. MP-SPR replicate run data for ICG liposome immobilization and the influence of sensor rejuvenation (20 °C, 50 µl/min, 670 nm for channel 1 and 2). Normalization of protein-to-liposome for each run is used to compensate for diminishing capacity to bind liposomes.

Liposome formulations

Table S1. Physicochemical characterization and endotoxin determination of ICG liposomes.				
	Hydrodynamic diameter (nm)	**Polydispersity index (PDI)**	**ζ-potential (mV)**	**Endotoxin**
Formulation 1 ICG(+) PEG(-)	120 ± 27	0.134	-1.42 ± 0.16	+++
Formulation 2 ICG(+) PEG(+)	121 ± 25	0.053	-1.90 ± 0.17	++
Formulation 3 ICG(-) PEG(+)	110 ± 20	0.050	-1.10 ± 0.44	+++

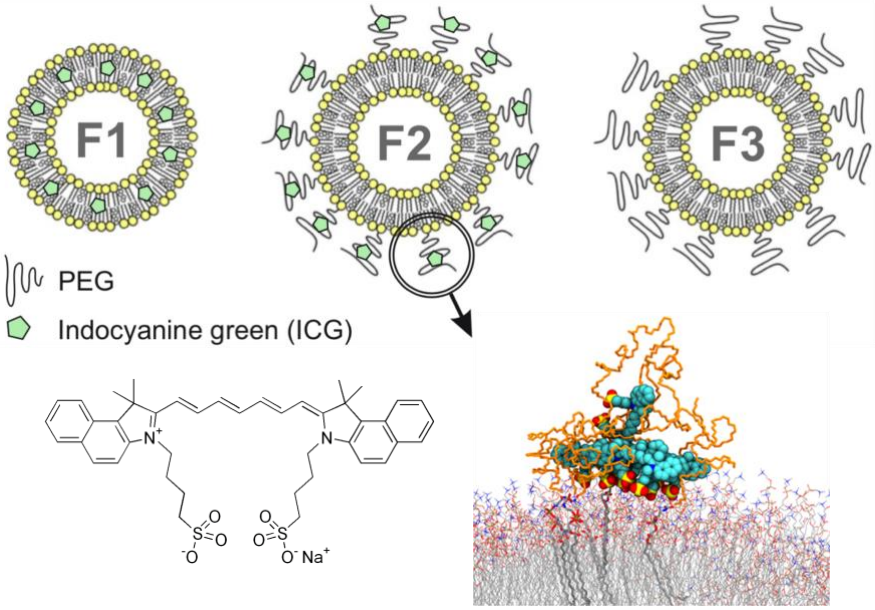

Figure S7. Light-triggered indocyanine green (ICG) liposome formulations F1 to F3 with the molecular structure of ICG and a molecular dynamics snapshot of clusters of ICG molecules with PEG (orange), modified

with permission[9]. F1: ICG(+) PEG (-); F2: ICG(+) PEG(+); F3: ICG(-)PEG(+). Liposome illustrations adapted from a publication by Frontiers under CC-BY 4.0[10].

Detection of ICG in MP-SPR

During immobilization, an increase exceeding 0.1 arbitrary units is consistently observed in the SPR peak minimum intensity in the full SPR angular scan curve measured at the 785 nm incident wavelengths of the SPR curve for F1 and F2, but not for F3 without ICG (**Figure S7**). These characteristic changes in the SPR peak minimum intensity measured at 785 nm can be attributed to the presence of ICG in the formulation, since the maximum absorption spectrum of ICG varies from 785 nm in monomeric state to 690 nm in aggregate state[11,12].

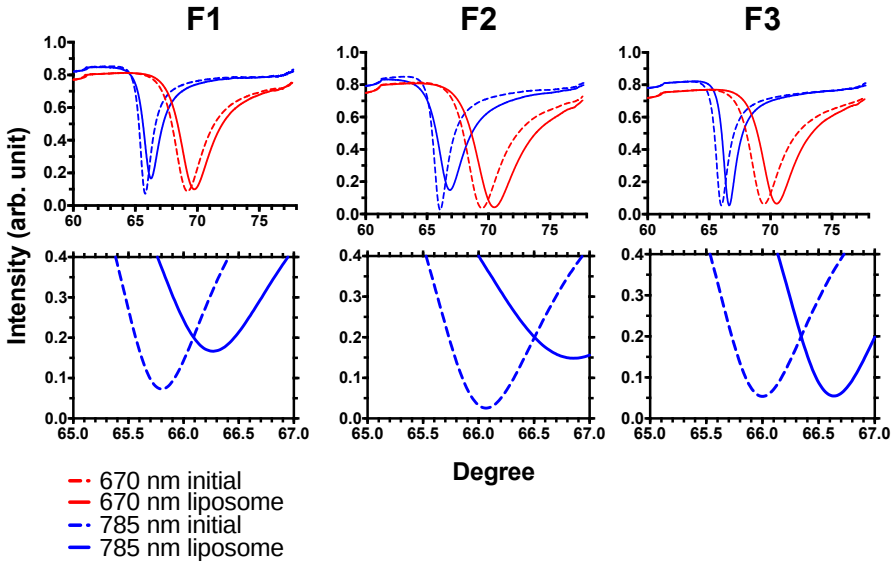

Figure S8. Top: Full SPR curves at 670 nm and 785 nm incident wavelength before (solid line) and after (dashed line) liposome immobilization for the measurement angular range of 60 to 78 degrees. **Bottom**: Comparison of 785 nm peak minima between 65 and 67 degrees. A characteristic and reproducible change in peak minimum angle intensity can be observed at 785 nm as a result ICG-containing liposome immobilization of F1 and F2, which is not observed with F3 without ICG.

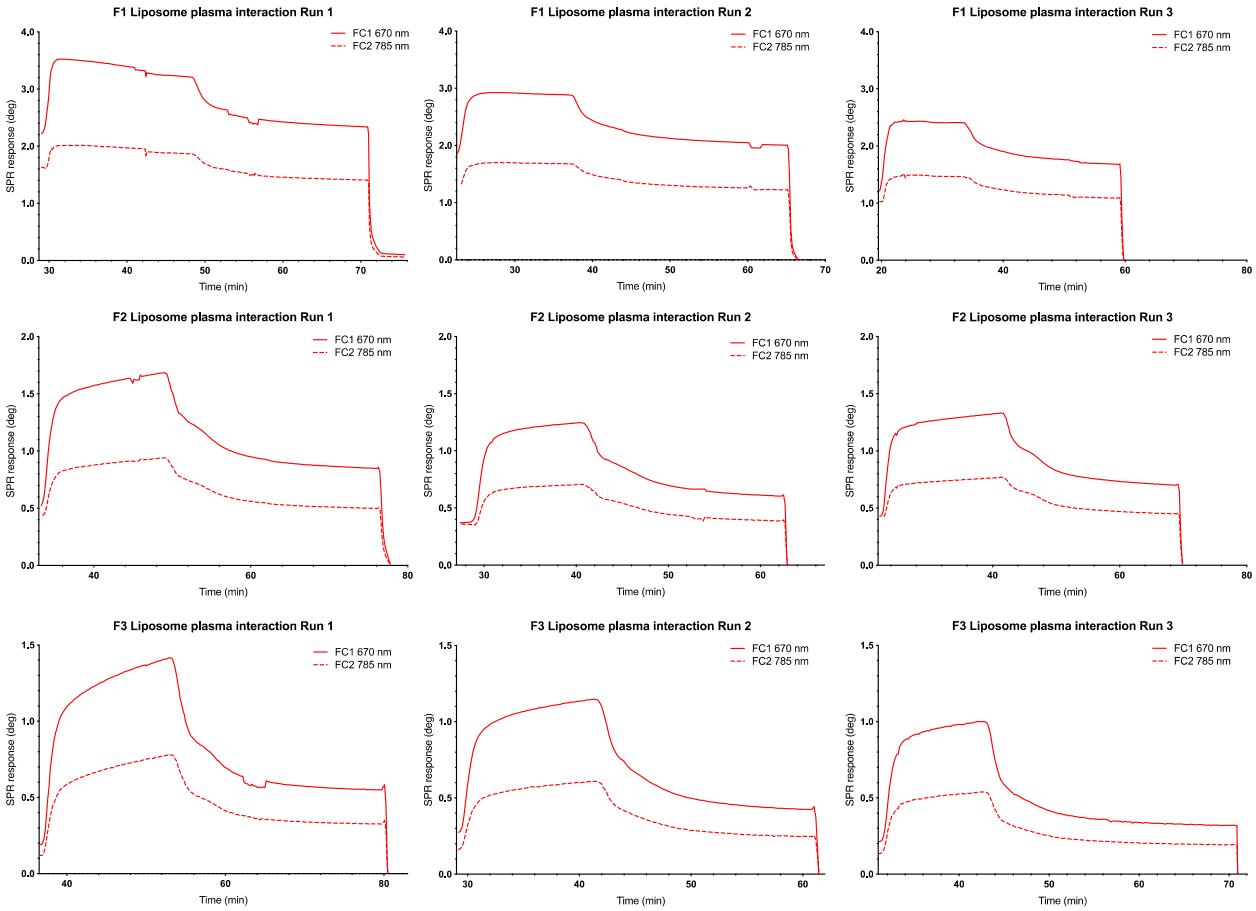

Figure S9. MP-SPR replicate run data for human plasma interaction from three measurements on dedicated rejuvenated sensor (20 °C, 50 µl/min, channel 1).

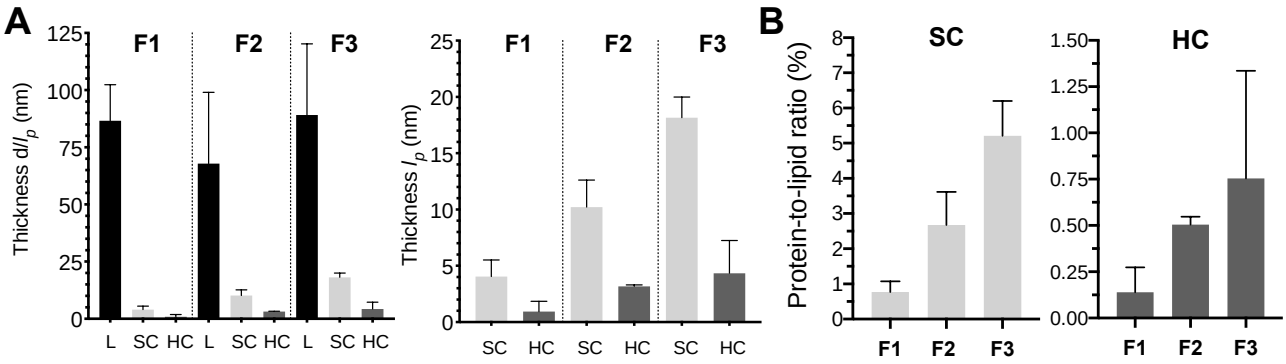

Figure S10 A: Comparison of liposome diameters (*d*) and the effective corona thicknesses (l_p) based on MP-SPR measurements: liposome (L), soft corona (SC), and hard corona (HC). The right side contains an enlarged snapshot with only the corona values. **B:** Corresponding protein-to-lipid ratios (%) that were used in the calculations to account for the different number of sensor-immobilized liposomes species between the formulations and measurement runs in the A panels.

Proteomics analysis

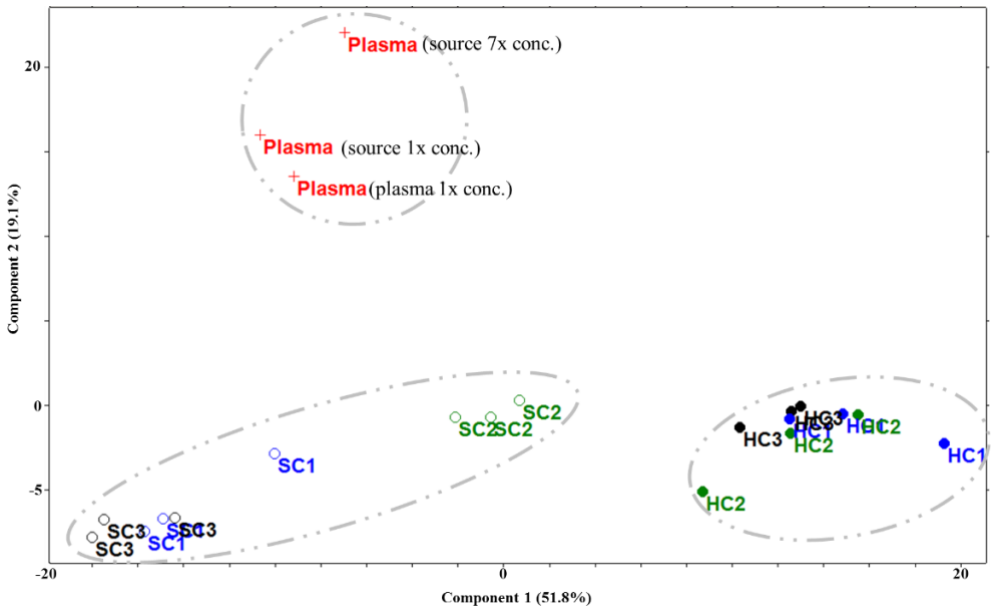

Figure S11. Top 2 components from PCA of all 189 identified plasma proteins. About 71% of the variation in protein abundance across all samples clusters the samples into three main groups corresponding to the SCs, HCs, and plasma (where 'plasma' refers to before injection and 'source' to plasma subjected to MP-SPR analysis as a control at 1-fold and 7-fold diluted). In addition, within the SC cluster, a very clear difference could be observed between F2 and formulations F1 and F3, which due to the distinct composition of SC2.

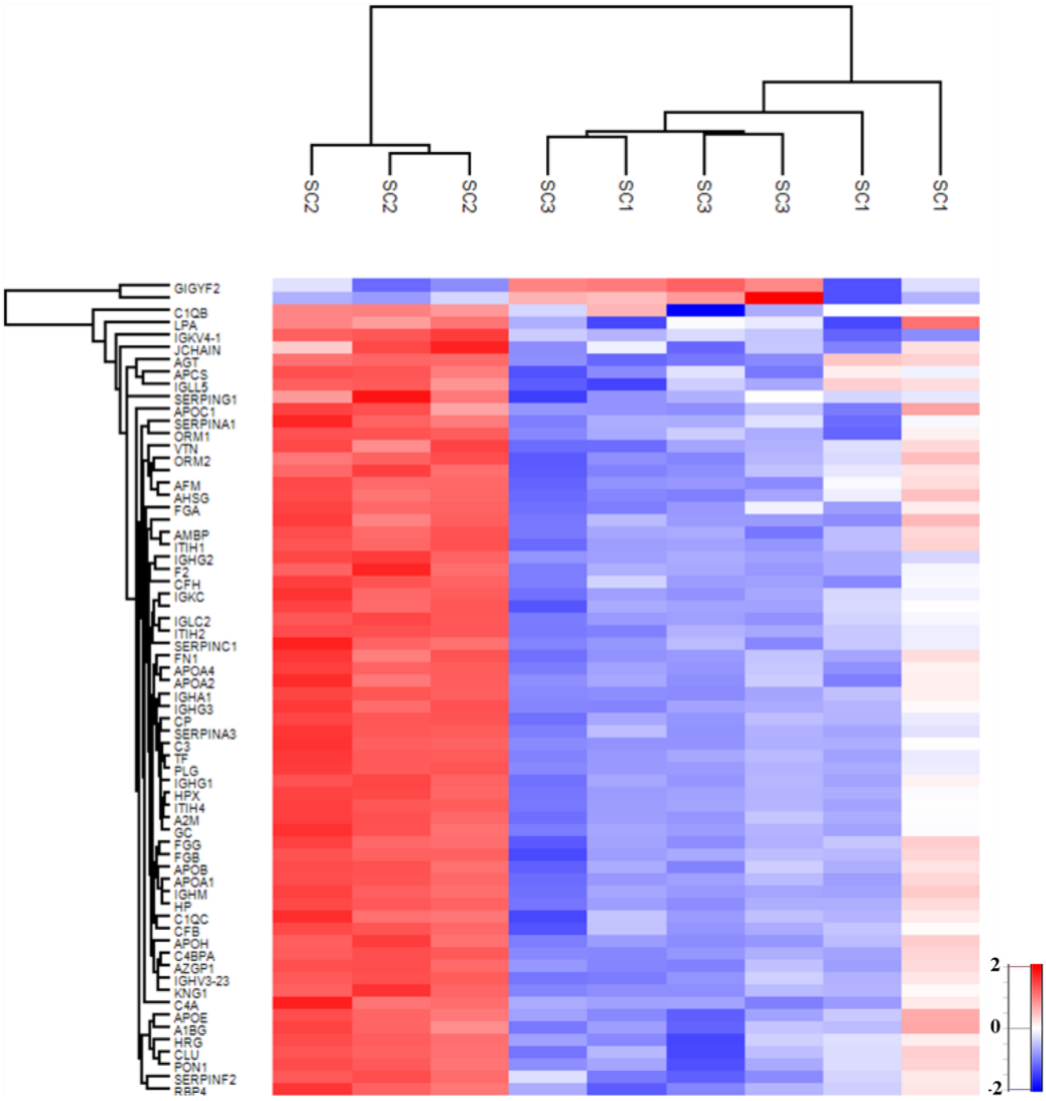

Figure S12. Formulation-dependent enrichment of proteins in SC enriched protein annotations and their biological functions. F2 surface enriches HC-type proteoforms in SC.

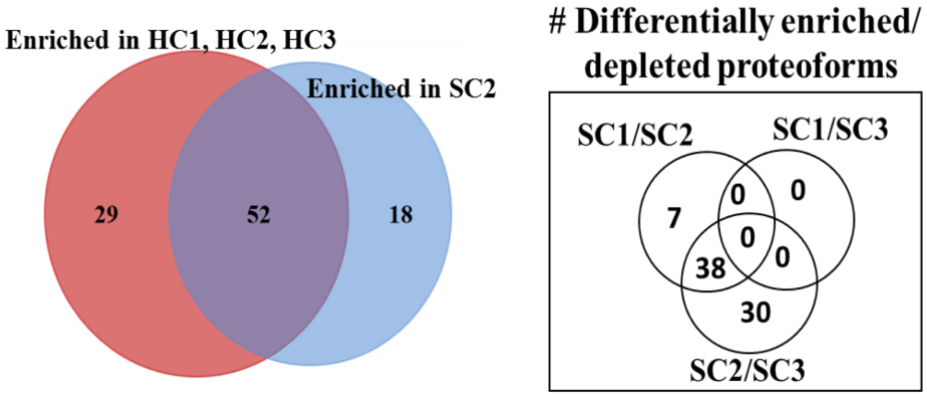

Figure S13. Venn diagrams of the differentially abundant proteoforms in HC and SC between the specified contrasts provided in Figure 8 and Supplementary Tables P1, P2, and P3. Clusterin is found depleted (-1.23-

fold) when the unpegylated SC1 is compared to pegylated SC2, along with several complement system components and immunoglobulins. The latter observation is expected since PEG has been shown to induce complement activation[13] and IgG and IgM antibodies against PEG have been reported on, albeit with some controversy[14,15]. Clusterin is significantly enriched in the soft corona of F2 (2.19-fold) together with apolipoprotein E (1.45-fold) comparing to SC3. Comparing SC2 to SC3, apolipoproteins C-I (3.25-fold), C-II (3.21-fold), L1 (2.25-fold), and B-100 (1.99-fold) are also found enriched, possibly as a result of ICG since both formulations were pegylated. Apolipoprotein A-I is also found significantly enriched in SC2 and present in other SCs, while also enriched in HCs overall (2.83-fold) when these are compared to SCs. However, in comparison with HCs, SC2 showed relative depletion of two apolipoproteins: clusterin and apolipoprotein C-III. Hemopexin, Immunoglobulin gamma-1, fibrinogen gamma, complement C3, apolipoproteins A-I and A-IV, alpha-1-antitrypsin, alpha-2-macroglobulin, and clusterin are found in the HC as a result of specific binding, as these were significantly depleted in the plasma.

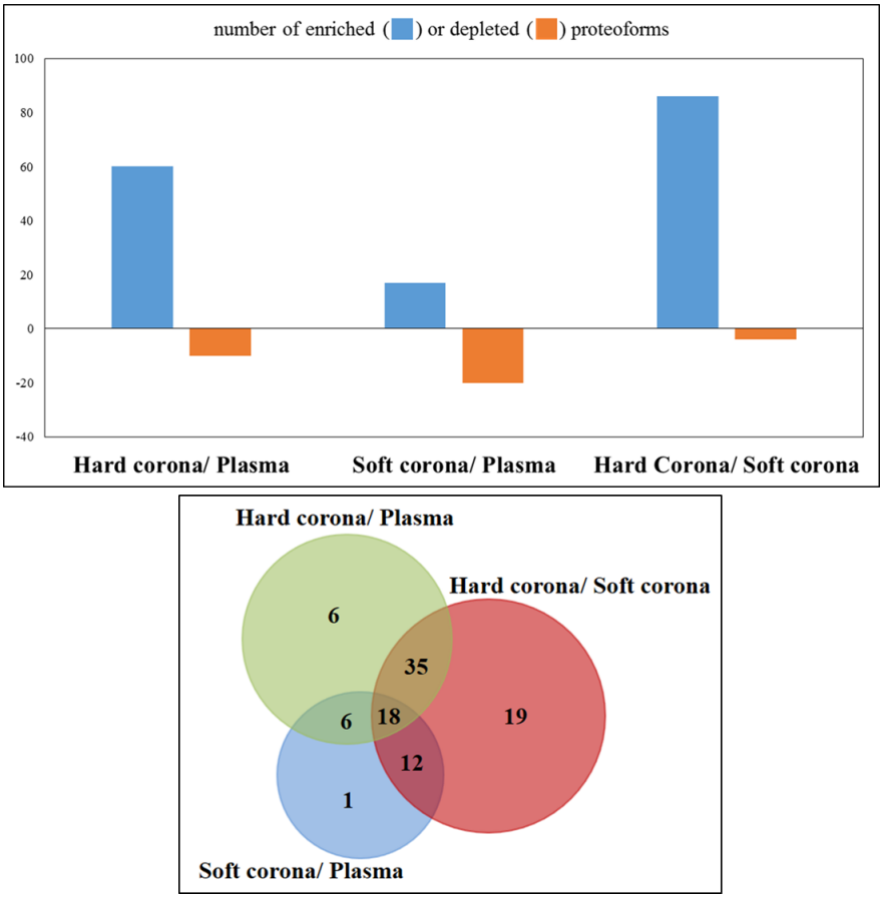

Figure S14. Enrichment of corona proteins relative to plasma source. To answer whether some proteins were bound to the liposome surfaces in a formulation-independent manner, abundance levels of hard and soft corona proteoforms were compared to each other (hard corona/ soft corona) as well as to the source plasma (hard corona/ plasma and soft corona/ plasma), irrespective of formulation type. All differentially enriched or depleted proteins, and their relative fold changes in abundance are listed in Supplementary Table P1.

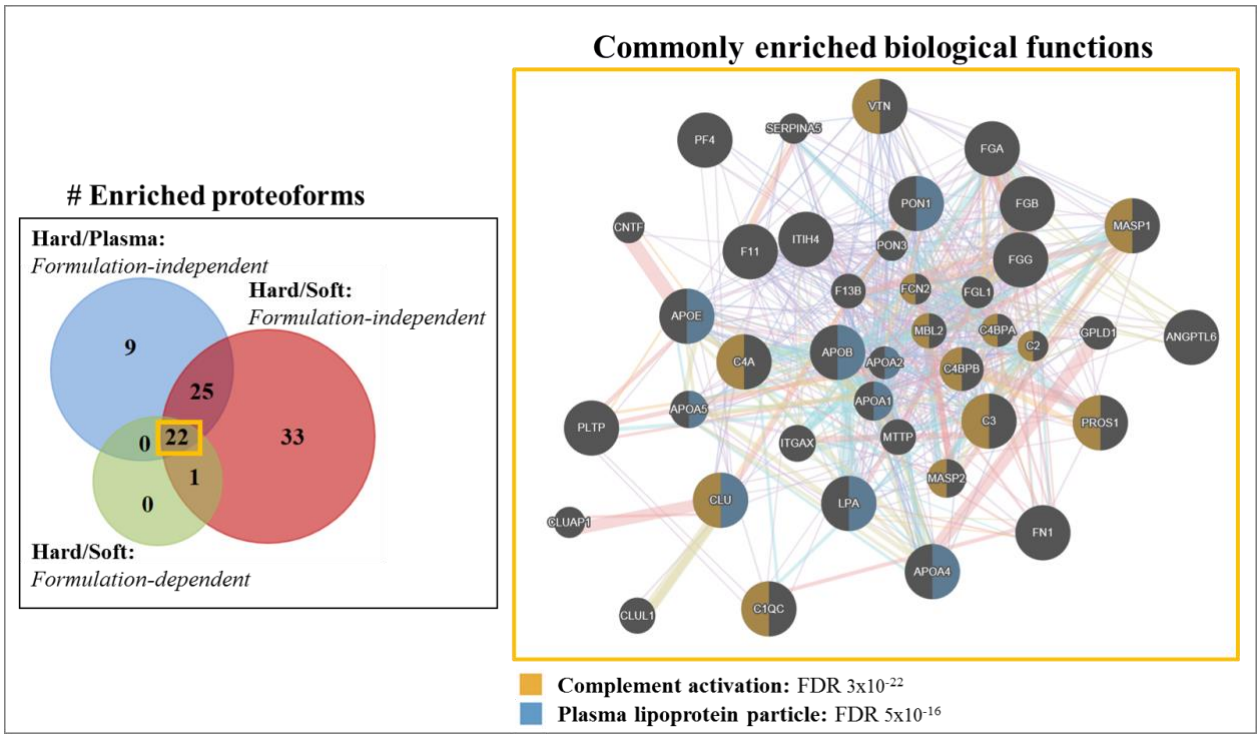

Figure S15. Plasma HC signature. The left panel depicts a Venn distribution of proteins that are significantly enriched in the HC fractions, when compared to plasma or SC fractions. That is, the overlapping enriched proteins from hard/soft corona comparisons for each formulation: HC1/SC1, HC2/SC2 and HC3/SC3 (green Venn), enriched proteins from all hard corona fractions grouped together compared to the source plasma (blue Venn) and enriched proteins from all hard corona fractions grouped together versus all SC fractions grouped together (red Venn). 22 proteins, corresponding to a HC signature were identified in all three groups. The top 2 biological functions represented by these core hard corona proteins were complement activation and plasma lipoprotein particle.

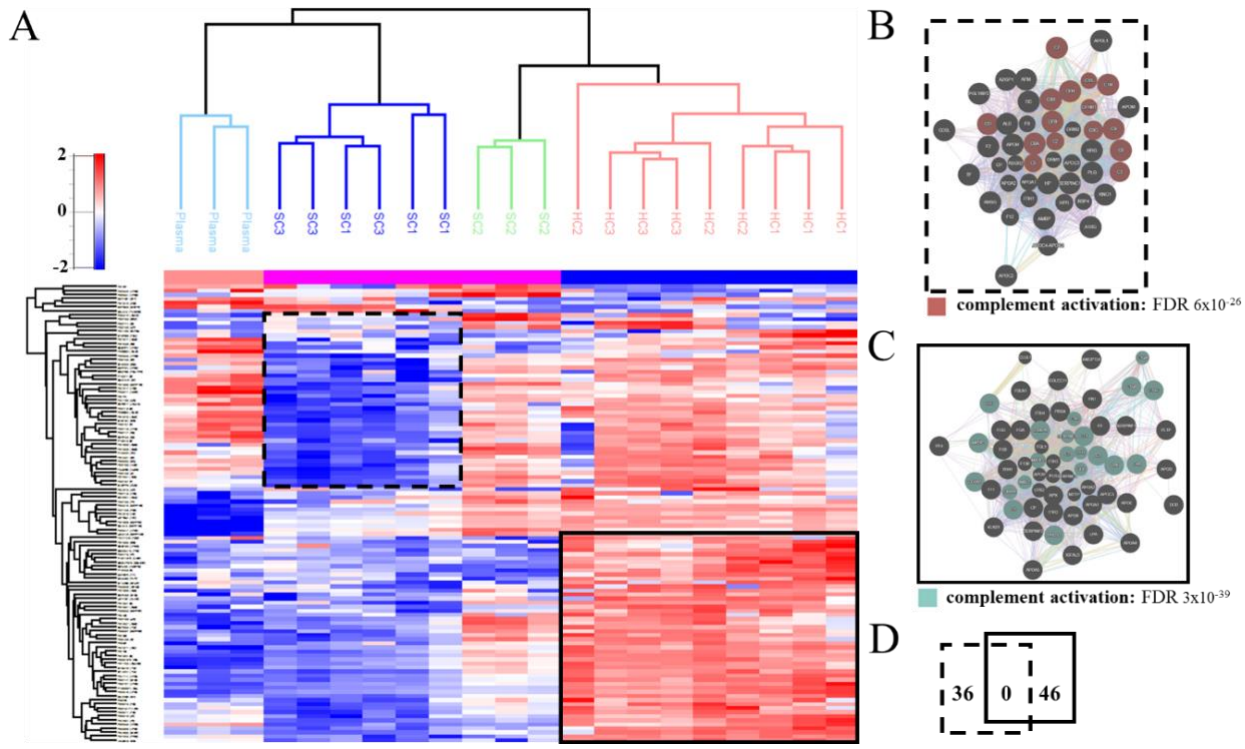

Figure S16. Multi-group ANOVA analysis: HC1, HC2, HC3, SC1, SC2, SC3, and plasma. Hierarchical cluster of proteins that are differentially abundant with respect to liposome formulation and corona type **(A)**. Four clusters corresponding to; *1.* Source plasma (Plasma), *2.* Soft corona; formulation F1 (SC1) and F3 (SC3), *3.* Soft corona; formulation F2 (SC2) and *4.* Hard corona formulation 1, 2 and 3 (HC1, HC2 and HC3) are highlighted with unique colours **(A)**. In addition, the protein groups identified as predominantly depleted in soft corona F1 and F3, relative to the source plasma (box with dashed outline) or predominantly enriched in hard corona fractions relative to source plasma only (box with solid outline), are also highlighted **(A)**. The most enriched biological functions, represented by these SC1/SC3 and HC1/HC2/HC3 signature proteoforms are depicted in **(B)** and **(C)** respectively. Venn comparisons **(D)** reveal that (although the same top biological function was enriched) the identified signature proteoforms were unique for the depleted in SC1/SC3 and enriched in HC1/HC2/HC3 categories.

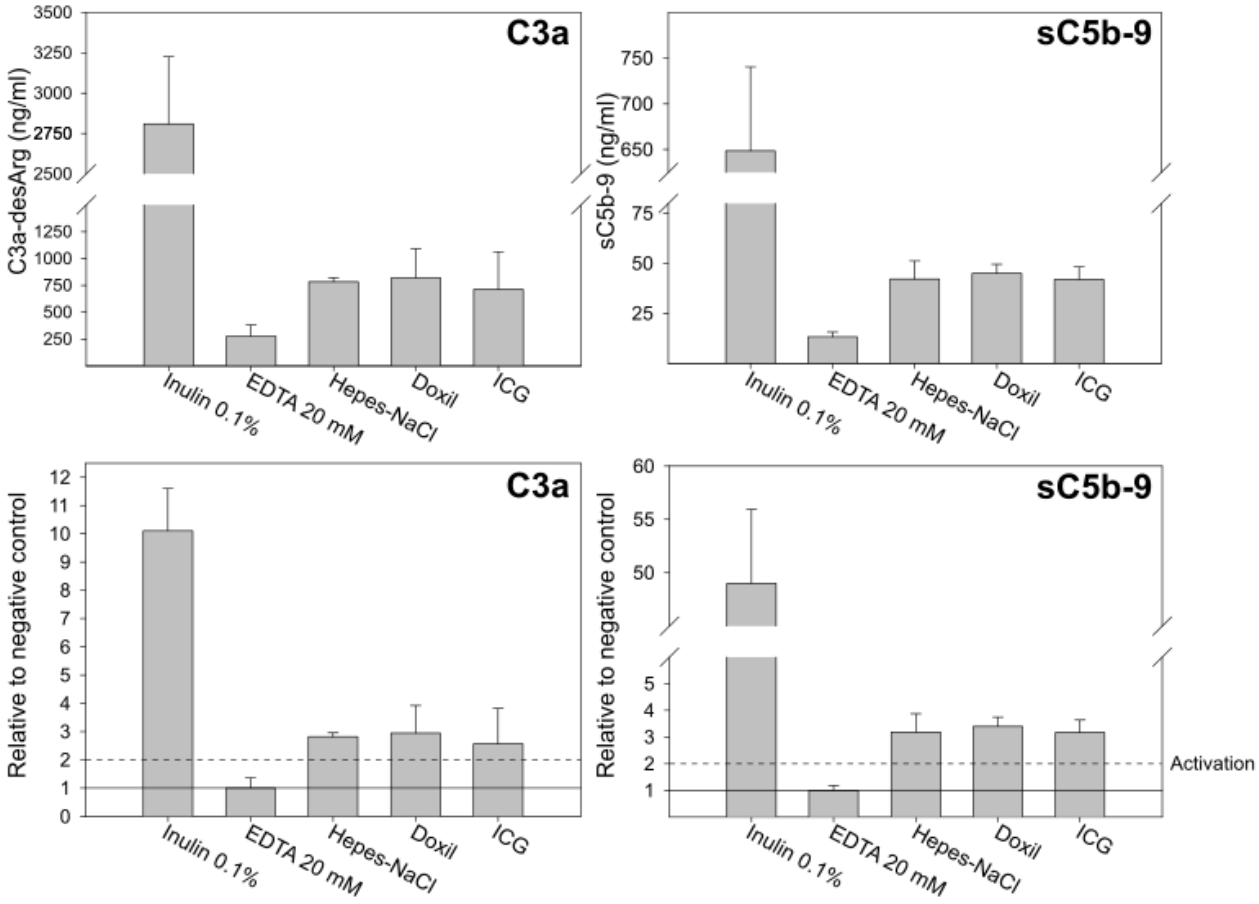

Figure S17. Complement activation by liposomes and controls. Data for C3a (left column) and sC5b-9 (right column) is presented as both absolute concentrations (ng/ml ± S.D.) on the top row and normalized to baseline negative control on the bottom row, where 2-fold or higher is considered activation[16]. Differences between samples were not statistically significant ($p>0.05$).

Minimum Information Reporting in Bio–Nano Experimental Literature

MINBE[17] (Minimum Information about Nanomaterial Biocorona Experiments) and MIRIBEL[18] reporting guidelines were consulted in the preparation of the manuscript.

The MIRIBEL guidelines were introduced here: https://doi.org/10.1038/s41565-018-0246-4

The development of these guidelines was led by the ARC Centre of Excellence in Convergent Bio-Nano Science and Technology: https://www.cbns.org.au/. Any updates or revisions to this document will be made available here: http://doi.org/10.17605/OSF.IO/SMVTF. This document is made available under a CC-BY 4.0 license: https://creativecommons.org/licenses/by/4.0/.

The MIRIBEL guidelines were developed to facilitate reporting and dissemination of research in bio–nano science. Their development was inspired by various similar efforts:

- MIAME (microarray experiments): *Nat. Genet.* **29** (2001), 365; http://doi.org/10.1038/ng1201-365
- MIRIAM (biochemical models): *Nat. Biotechnol.* **23** (2005) 1509; http://doi.org/10.1038/nbt1156

- MIBBI (biology/biomedicine): *Nat. Biotechnol.* **26** (2008) 889; http://doi.org/10.1038/nbt.1411
- MIGS (genome sequencing): *Nat. Biotechnol.* **26** (2008) 541; http://doi.org/10.1038/nbt1360
- MIQE (quantitative PCR): *Clin. Chem.* **55** (2009) 611; http://doi.org/10.1373/clinchem.2008.112797
- ARRIVE (animal research): *PLOS Biol.* **8** (2010) e1000412; http://doi.org/10.1371/journal.pbio.1000412
- *Nature*'s reporting standards:
    - Life science: https://www.nature.com/authors/policies/reporting.pdf; e.g., *Nat. Nanotechnol.* **9** (2014) 949; http://doi.org/10.1038/nnano.2014.287
    - Solar cells: https://www.nature.com/authors/policies/solarchecklist.pdf; e.g., *Nat. Photonics* **9** (2015) 703; http://doi.org/10.1038/nphoton.2015.233
    - Lasers: https://www.nature.com/authors/policies/laserchecklist.pdf; e.g., *Nat. Photonics* **11** (2017) 139; http://doi.org/10.1038/nphoton.2017.28
- The "TOP guidelines": e.g., *Science* **352** (2016) 1147; http://doi.org/10.1126/science.aag2359

Similar to many of the efforts listed above, the parameters included in this checklist are **not** intended to be definitive requirements; instead they are intended as 'points to be considered', with authors themselves deciding which parameters are—and which are not—appropriate for their specific study.

This document is intended to be a living document, which we propose is revisited and amended annually by interested members of the community, who are encouraged to contact the authors of this document. Parts of this document were developed at the annual International Nanomedicine Conference in Sydney, Australia: http://www.oznanomed.org/, which will continue to act as a venue for their review and development, and interested members of the community are encouraged to attend.

After filling out the following pages, this checklist document can be attached as a "Supporting Information" document during submission of a manuscript to inform Editors and Reviewers (and eventually readers) that all points of MIRIBEL have been considered.

Supplementary Table 1. Material characterization*

Question	Yes	No
1.1 Are "**best reporting practices**" **available** for the nanomaterial used? For examples, see *Chem. Mater.* **28** (2016) 3535; http://doi.org/10.1021/acs.chemmater.6b01854 and *Chem. Mater.* **29** (2017) 1; http://doi.org/10.1021/acs.chemmater.6b05235	x	
1.2 If they are available, **are they used**? If not available, ignore this question and proceed to the next one.	x	
1.3 Are extensive and clear instructions reported detailing all steps of **synthesis** and the resulting **composition** of the nanomaterial? For examples, see *Chem. Mater.* **26** (2014) 1765; http://doi.org/10.1021/cm500632c, and *Chem. Mater.* **26** (2014) 2211; http://doi.org/10.1021/cm5010449. Extensive use of photos, images, and videos are strongly encouraged. For example, see *Chem. Mater.* **28** (2016) 8441; http://doi.org/10.1021/acs.chemmater.6b04639	x	
1.4 Is the **size** (or **dimensions**, if non-spherical) and **shape of** the nanomaterial reported?	x	
1.5 Is the **size dispersity** or **aggregation** of the nanomaterial reported?	x	
1.6 Is the **zeta potential** of the nanomaterial reported?	x	

1.7 Is the **density (mass/volume)** of the nanomaterial reported?	x	
1.8 Is the amount of any **drug loaded** reported? 'Drug' here broadly refers to functional cargos (e.g., proteins, small molecules, nucleic acids).	N/A	
1.9 Is the **targeting performance** of the nanomaterial reported, including **amount** of ligand bound to the nanomaterial if the material has been functionalised through addition of targeting ligands?	N/A	
1.10 Is the **label signal** per nanomaterial/particle reported? For example, fluorescence signal per particle for fluorescently labelled nanomaterials.	N/A	
1.11 If a material property not listed here is varied, has it been **quantified**?	x	
1.12 Were characterizations performed in a **fluid mimicking biological conditions**?	x	
1.13 Are details of how these parameters were **measured/estimated** provided?	x	
Explanation for **No** (if needed):		

***Ideally, material characterization should be performed in the same biological environment as that in which the study will be conducted. For example, for cell culture studies with nanoparticles, characterization steps would ideally be performed on nanoparticles dispersed in cell culture media. If this is not possible, then characteristics of the dispersant used (e.g., pH, ionic strength) should mimic as much as possible the biological environment being studied.

Supplementary Table 2. Biological characterization*

Question	Yes	No
2.1 Are **cell seeding details**, including **number of cells plated, confluency at start of experiment,** and **time between seeding and experiment** reported?	N/A	
2.2 If a standardised cell line is used, are the **designation and source** provided?	N/A	
2.3 Is the **passage number** (total number of times a cell culture has been subcultured) known and reported?	N/A	
2.4 Is the last instance of **verification of cell line** reported? If no verification has been performed, is the time passed and passage number since acquisition from trusted source (e.g., ATCC or ECACC) reported? For information, see *Science* **347** (2015) 938; http://doi.org/10.1126/science.347.6225.938	N/A	
2.5 Are the results from **mycoplasma testing** of cell cultures reported?	N/A	
2.6 Is the **background signal of cells/tissue** reported? (E.g., the fluorescence signal of cells without particles in the case of a flow cytometry experiment.)	N/A	
2.7 Are **toxicity studies** provided to demonstrate that the material has the expected toxicity, and that the experimental protocol followed does not?	x	
2.8 Are details of media preparation (**type of media, serum,** any **added antibiotics**) provided?	N/A	
2.9 Is a **justification of the biological model** used provided? For examples for cancer models, see *Cancer Res.* **75** (2015) 4016; http://doi.org/10.1158/0008-5472.CAN-15-1558, and *Mol. Ther.* **20** (2012) 882; http://doi.org/10.1038/mt.2012.73, and *ACS Nano* **11** (2017) 9594; http://doi.org/10.1021/acsnano.7b04855	N/A	
2.10 Is characterization of the **biological fluid** (*ex vivo*/*in vitro*) reported? For example, when investigating protein adsorption onto nanoparticles dispersed in blood serum, pertinent aspects of the blood serum should be characterised (e.g., protein concentrations and differences between donors used in study).		x

2.11 For **animal experiments**, are the ARRIVE guidelines followed? For details, see *PLOS Biol.* **8** (2010) e1000412; http://doi.org/10.1371/journal.pbio.1000412	N/A	
Explanation for **No** (if needed): **Comment on 2.10:** Research-use-only FFP24 (fresh frozen plasma within 24 hours) obtained from the local blood service was used in the study. Donor details, including gender and age, are anonymized by the supplier. A relative enrichment analysis was performed using label-free LC-MS/MS, which compares the protein amount in the corona subsection to its amount in the source plasma. The plasma total protein concentration is reported.		

*For *in vitro* experiments (e.g., cell culture), *ex vivo* experiments (e.g., in blood samples), and *in vivo* experiments (e.g., animal models). The questions above that are appropriate depend on the type of experiment conducted.

Supplementary Table 3. Experimental details*

Question	Yes	No
3.1 For cell culture experiments: are **cell culture dimensions** including **type of well**, **volume of added media**, reported? Are cell types (i.e.; adherent vs suspension) and **orientation** (if non-standard) reported?	N/A	
3.2 Is the **dose of material administered** reported? This is typically provided in nanomaterial mass, volume, number, or surface area added. Is sufficient information reported so that regardless of which one is provided, the other dosage metrics can be calculated (i.e. using the dimensions and density of the nanomaterial)?	N/A	
3.3 For each type of imaging performed, are details of how **imaging** was performed provided, including details of **shielding, non-uniform image processing**, and any **contrast agents** added?	N/A	
3.4 Are details of how the dose was administered provided, including **method of administration, injection location, rate of administration,** and details of **multiple injections**?	N/A	
3.5 Is the methodology used to **equalise dosage** provided?	N/A	
3.6 Is the **delivered dose** to tissues and/or organs (in vivo) reported, as % injected dose per gram of tissue (%ID g^{-1})?	N/A	
3.7 Is **mass of each organ/tissue measured** and **mass of material** reported?	N/A	
3.8 Are the **signals of cells/tissues with nanomaterials** reported? For instance, for fluorescently labelled nanoparticles, the total number of particles per cell or the fluorescence intensity of particles + cells, at each assessed timepoint.	N/A	
3.9 Are **data analysis details**, including **code used** for analysis provided?	x	
3.10 Is the **raw data** or **distribution of values** underlying the reported results provided? For examples, see *R. Soc. Open Sci.* **3** (2016) 150547; http://doi.org/10.1098/rsos.150547, https://opennessinitiative.org/making-your-data-public/, http://journals.plos.org/plosone/s/data-availability, and https://www.nature.com/sdata/policies/repositories	x	
Explanation for **No** (if needed):		

* The use of protocol repositories (e.g., *Protocol Exchange* http://www.nature.com/protocolexchange/) and published standard methods and protocols (e.g., *Chem. Mater.* **29** (2017) 1;

http://doi.org/10.1021/acs.chemmater.6b05235, and *Chem. Mater.* **29** (2017) 475; http://doi.org/10.1021/acs.chemmater.6b05481) are encouraged.

References

1 L. S. Jung, C. T. Campbell, T. M. Chinowsky, M. N. Mar and S. S. Yee, *Langmuir*, 1998, **14**, 5636–5648.
2 D. L. M. Rupert, G. V. Shelke, G. Emilsson, V. Claudio, S. Block, C. Lässer, A. Dahlin, J. O. Lötvall, M. Bally, V. P. Zhdanov and F. Höök, *Anal. Chem.*, 2016, **88**, 9980–9988.
3 A. Mashaghi, M. Swann, J. Popplewell, M. Textor and E. Reimhult, *Anal. Chem.*, 2008, **80**, 3666–3676.
4 R. M. Murphy and C. C. Lee, in *Misbehaving Proteins: Protein (Mis)Folding, Aggregation, and Stability*, Springer New York, New York, NY, 2006, pp. 147–165.
5 N. Granqvist, M. Yliperttula, S. Välimäki, P. Pulkkinen, H. Tenhu and T. Viitala, *Langmuir*, 2014, **30**, 2799–2809.
6 W. M. Albers, T. Munter, P. Laaksonen and I. Vikholm-Lundin, *J. Colloid Interface Sci.*, 2010, **348**, 1–8.
7 I. Vikholm-Lundin, R. Piskonen and W. M. Albers, *Biosens. Bioelectron.*, 2007, **22**, 1323–1329.
8 A. Olaru, M. Gheorghiu, S. David, C. Polonschii and E. Gheorghiu, *Biosens. Bioelectron.*, 2013, **45**, 77–81.
9 T. Lajunen, L.-S. Kontturi, L. Viitala, M. Manna, O. Cramariuc, T. Róg, A. Bunker, T. Laaksonen, T. Viitala, L. Murtomäki and A. Urtti, *Mol. Pharm.*, 2016, **13**, 2095–2107.
10 J. R. Ashton, J. L. West and C. T. Badea, *Front. Pharmacol.*, 2015, 6, 256.
11 M. L. Landsman, G. Kwant, G. A. Mook and W. G. Zijlstra, *J. Appl. Physiol.*, 1976, **40**, 575–583.
12 J. F. Zhou, *Proc. SPIE*, 1994, **2128**, 495–505.
13 I. Hamad, O. Al-Hanbali, A. C. Hunter, K. J. Rutt, T. L. Andresen and S. M. Moghimi, *ACS Nano*, 2010, **4**, 6629–6638.
14 H. Schellekens, W. E. Hennink and V. Brinks, *Pharm. Res.*, 2013, **30**, 1729–1734.
15 T. Ishida, R. Maeda, M. Ichihara, K. Irimura and H. Kiwada, *J. Control. Release*, 2003, **88**, 35–42.
16 M. A. Dobrovolskaia and B. W. Neun, *Nanotechnol. Charact. Lab. Natl. Cancer Institute-Frederick*, 2010, 1–10.
17 A. J. Chetwynd, K. E. Wheeler and I. Lynch, *Nano Today*, 2019, **28**, 100758.
18 M. Faria, M. Björnmalm, K. J. Thurecht, S. J. Kent, R. G. Parton, M. Kavallaris, A. P. R. Johnston, J. J. Gooding, S. R. Corrie, B. J. Boyd, P. Thordarson, A. K. Whittaker, M. M. Stevens, C. A. Prestidge, C. J. H. Porter, W. J. Parak, T. P. Davis, E. J. Crampin and F. Caruso, *Nat. Nanotechnol.*, , DOI:10.1038/s41565-018-0246-4.